[AMERICAN JOURNAL OF SCIENCE, VOL. 293, FEBRUARY, 1993, P. 111–134]

SECONDARY-MINERAL FORMATION DURING NATURAL WEATHERING OF PYROXENE: REVIEW AND THERMODYNAMIC APPROACH

Y. NOACK*, F. COLIN**, D. NAHON*, J. DELVIGNE**, and L. MICHAUX*

Géosciences de l'Environnement-URA CNRS 132, Université AIX-Marseille III, Case 431, Faculté des Sciences et Techniques de St Jérôme, 13397 Marseille Cedex 13, France

ABSTRACT. Physical and chemical factors controlling natural weathering processes of pyroxenes through the formation of secondary minerals are reviewed. It has been shown that besides climate, mineralogy, and petrology of parent rocks, mineralogy and structural arrangement of secondary phases rule over the composition of the pyroxene-derived products during increased weathering. Drainage conditions, however, are the most critical factors in constraining weathering paths from the earlier stages of cation-depleted layer-silicate formation to the last stages of goethite/kaolinite formation. A succession of transitional phyllosilicates develops from Mg-endmembers to Fe- or Al-endmembers. The chemistry of natural percolating waters remains poorly known, and local pH and Eh are generally unknown and difficult to measure in situ. Nevertheless these agents should play an important role at the microscale in the formation of weathering products. Therefore, thermodynamic simulation is required for a better understanding of the natural secondary products formed at the expense of pyroxene. In this paper, computerized calculations were used to monitor the theoretical congruent dissolution, without kinetic effects, of a known mixture of minerals with a solution defined by initial pH, O_2, and CO_2 fugacities, temperature, and opening degree of the system. Results of this thermodynamic modeling generally agree with natural weathering paths, as, for example, successive replacements of pyroxene by Fe- and Al-bearing products such as goethite, kaolinite, and smectites. Changes of pO_2 and Al-content strongly control the composition of the clay solid-solution. Consideration of kinetic effects, composition of weathering solutions in the field, and in situ oxygen fugacity measurement should rank high among future research priorities.

INTRODUCTION

Pyroxene weathering has been the subject of numerous studies (Smith, 1962; Delvigne, 1965, 1983, 1990; Hendricks and Whittig, 1968a, 1968b; Loughnan, 1969; Basham, 1974; Eswaran, 1979; Eggleton and Boland, 1982; Nahon and Colin, 1982; Colin and others, 1985; De Kimpe, Dejou and Chevalier, 1987; Velbel, 1987; Colin and others, 1990). Weathering has been investigated by unravelling petrological, mineralogical, and chemical paths from fresh rocks to derived soils, either vertically through single pit profile or laterally through sequential

** ORSTOM, 213, Rue Lafayette, 75480 Paris Cedex 10, France.

upslope to downslope pit profiles. Physical and chemical factors controlling weathering processes of pyroxenes were considered such as mineralogy and petrology of parent rocks (pyroxenite, peridotite, gabbro, basalt), climate (equatorial to cold), drainage conditions (open to closed system, pore type and size, lateral or vertical water potential), mineralogy and structural arrangement of secondary phases (phyllosilicates and iron oxi-hydroxides, texture and structure, see table 1). Mechanisms of dissolution and their corresponding rates were experimentally determined and calculated (Luce, Bartlett, and Parks, 1972; Grandstaff, 1977; Siever and Woodford, 1979; Schott, Berner, and Sjoberg, 1981; Schott and Berner, 1983; Velbel, 1987; . . .).

In contrast to the abundant mineralogical data on the weathering of pyroxenes, no accurate data exist in the literature on weathering solutions, and the chemistry of percolating water remains little known in spite of its important microscale role in the generated of weathering products. Whereas the chemistry of rain waters, river waters, and groundwaters can be analyzed easily, this is not the case for the solutions of active weathering microsites, because they may vary significantly over a few microns in response to permeability increase, drainage modification, and leaching solution chemistry and hence undergo major changes (Glasmann and Simonson, 1985; De Kimpe, Dejou, and Chevalier, 1987). In addition, unlike hydrothermal alteration, no fluid inclusion can be used as temperature or solution chemistry indicators in weathering. The behavior of stable and unstable isotope in weathering products remains poorly understood and is an unsatisfactory expression of reflecting the physico-chemical conditions of weathering (Pavich and others, 1984, 1986; Noack, Decarreau, and Manceau, 1986; Savin and Lee, 1988). Chemical compositions of weathering solutions can be determined only indirectly by experimental work based on the chemistry of primary minerals and under different temperatures, partial gas pressures, and pH. Because silicate weathering rates are low under natural conditions, laboratory experiments must often use increased temperatures or extreme pHs to produce detectable rates on experimental time scales, thus strongly limiting the applicability of the results to natural conditions.

Following Helgeson, Garrels, and Mackenzie (1969), and Helgeson and others (1970), computerized models were applied to simulate geochemical processes with separately or simultaneously modified parameters (Fritz, 1975, 1981; Wolery and Walters, 1975). According to these models, reaction time can be estimated by introducing kinetic coefficients (Madé, Clement, and Fritz, 1990). However, difficulties in obtaining refined thermodynamic data and in comparing the calculated simulation with natural systems show the limitation of such models. The evolutionary models, however, are useful tools in understanding weathering solution paths and in estimating the corresponding physico-chemical conditions.

The present study reviews mineralogical, petrographical, and chemical data concerning the weathering of pyroxenes and proposes a thermo-

TABLE 1

Literature data on pyroxene weathering

References	Country	Type of Rocks	Climate	Transformation of Pyroxenes
Smith, 1962	Scotland	Basic igneous rocks	5–16°C, 750–900 mm	AUG → Fe-hydroxides → Clay Minerals AUG → Clay Minerals
Delvigne, 1965	Ivory Coast	Gabbro and Dolerite	Tropical 1200 to 2000 mm	AUG → Fe-hydroxides → Goethite HYP → Fe- hydroxides → Goethite + Voids ENS and DIOP → Fe-hydroxides → Goethite + Voids ENS and DIOP → Chlorite-Vermiculite + (Fe-hydroxides)
Hendricks and Whittig, 1968	USA	Andesite	Submediterranean elevation of 2000 m	HYP → Fe-hydroxides → Clay Minerals
Basham, 1974	Scotland	Gabbro	Submediterranean	AUG → Vermiculite + Fe-hydroxides + Voids HYP → Vermiculite + (Fe-hydroxides)
Trescases, 1975	N-Caledonie	Peridotite	Tropical 17°C, 1700 mm	ENS → Talc + (Quartz) + (Chlorite) → Goethite + Fe-hydroxides
Wackermann, 1975	Senegal	Gabbro	28°C, 1000–1500 mm	PX → Vermiculite + Goethite
Pion, 1979	Burkina Faso	Gabbro	16–40°C, 550 mm	HYP → Smectite HYP → Kaolinite + Goethite
Eswaran, 1979	Malaysia	Andesitic Basalts	27°C, 2500 mm	AUG → Fe-hydroxides → Goethite AUG → Montmorillonite → Goethite
Nahon and Colin, 1982	Ivory Coast	Pyroxenite	Tropical, 1600 mm	OPX → Amorphous → Clay Minerals → Fe-hydroxides
Nahon et al., 1982	Ivory Coast	Pyroxenite	Tropical, 1600 mm	PX → Amorphous → Talc + (Smectites) → Fe-hydroxides
Glasmann, 1982	USA	Andesite	10°C, 2000–2200 mm	AUG → Smectites + Voids
Delvigne, 1983	Ivory Coast	Pyroxenite		CPX → Amorphous → Smectites → Smectites + Fe-hydroxides + Voids → Amorphous → Kaolinite OPX → Smectites → Smectites + Fe-hydroxides + Voids
Fontanaud and Meunier, 1983	France	Lherzolite	Temperate	OPX → Talc → Saponite → Gel + Nontronite
Colin, 1984	Brazil	Pyroxenite	24°C, 1200–1800 mm	PX → Amorphous → Smectites → Kaolinite + Goethite
Glasmann and Simonson, 1985	USA	Basalt	10°C, 1800–2000 mm	AUG → Smectites + Goethite
Ildefonse, 1987	France Cameroun	Basalt Basalt	Temperate	Salite → Fe-hydroxides + Smectites + Voids Salite → Goethite + Anatase
De Kimpe et al., 1987	Canada	Pyroxenite	Temperate	AUG = Smectites
De Oliveira and Delvigne, 1988	Brazil	Pyroxenite	Tropical	AUG → Smectites → Goethite + Kaolinite

dynamic approach to the understanding and prediction of pyroxene weathering.

REVIEW OF NATURAL WEATHERING OF PYROXENES

In this part, mineralogical, petrological, and chemical data from the literature on weathering of pyroxenes were combined with an approach including gradual stages of weathering and different factors controlling weathering processes. The first stages of weathering were studied either experimentally or by using electron microscopy. Phyllosilicate and oxide stages were considered consequences of the changes of control factors such as primary mineralogy, climate, drainage intensity, and redox conditions.

First Stages of Weathering

Corrosion features either observed on natural pyroxene grains picked out from deep weathering layers and soil samples or obtained experimentally by acid attack of fresh grains clearly showed that dissolution does not affect the entire surface of pyroxenes. Hydrolysis reactions occurred at high surface energy sites such as grain edges and corners, cracks, point defects, twin boundaries, and dislocations (Schott, Berner, and Sjoberg, 1981; Berner and others, 1980; Berner and Schott, 1982; Schott and Berner, 1985).

Experimental dissolution of pyroxenes at room temperature and pH 6 consisted, in the early stages, of a non-stoichiometric release of Ca, Mg, and Si (Schott, Berner, and Sjoberg, 1981; Berner and Schott, 1982; Schott and Berner, 1985). For enstatite, the mass loss of Mg was greater than the Si loss. For diopside, Ca was preferentially released in relation to Mg and Si, with a constant Mg/Si ratio. For augite, Mg seemed released preferentially to Ca (Berner and Schott, 1982; Lartigue and others, 1991). At pH 1 and at room temperature, dissolution effects were similar to those obtained at pH 6, but reactions went faster. Released cations were substituted either by H^+ or H_3O^+ in the outer 10 Å of the grains, the so-called "protonated surface." The constant thickness of these protonated surfaces, while dissolution proceeded, demonstrated that this dissolution was congruent (Berner and Schott, 1982; Lartigue and others, 1991).

Using Resonant Nuclear Reactions, Petit and others (1987) concluded that during diopside weathering, penetrating hydrogens occurred partly as molecular water. The surficial defect density played a major role in water diffusion up to a depth of a few hundred Å. Mogk and Locke (1988) obtained similar results by applying Auger Electron Spectroscopy to the natural weathering of another type of chain-silicates. Ca and Mg were preferentially leached out in comparison with Si and Fe up to depths of nearly 500 Å beneath the mineral surface.

Using the petrographic microscope and the scanning electron microscope (SEM) with energy dispersive capability, Nahon and Colin (1982) identified amorphous products at the rims of slightly weathered py-

roxenes extracted from the base of the Sipilou weathering profile in the Ivory Coast. These products were slightly Mg-depleted compared to the fresh pyroxenes, and texturally well differentiated from the parental pyroxene. Similar amorphous products were found to be early weathering stages of clinopyroxenes from gabbros in Scotland (Basham, 1974) and from pyroxenites in the Ivory Coast (Delvigne, 1983). These slightly Ca and/or Mg-depleted phases seemed to occur at the "surface" of pyroxenes and sometimes became sufficiently well developed to be seen under the petrographic microscope (Colin and others, 1985). Such amorphous materials could be interpreted as mature products resulting from development of a preceding "hydrated layer" or "protonated surface" which still belonged to the parent mineral and was resistant to ultrasonic treatment. Amorphous phases were well expressed in closed weathering systems such as saprolite, near the water table or downslope profiles (Nahon and Colin, 1982; Delvigne, 1983).

Phyllosilicates and Oxide Stages

The next stages with increased weathering of pyroxenes under lateritic conditions were the complete dissolution of parent minerals and their replacement by phyllosilicates and/or iron oxihydroxides. Primary mineralogy, climate, drainage intensity, redox conditions, and pH controlled texture and chemical composition of the weathering products.

The parent mineral.—Although data in literature are scarce, orthopyroxene (OPX) apparently weathers faster than clinopyroxene (CPX) under similar conditions, and the resulting weathering products may or may not vary with different parent minerals. Eggleton (1986) suggested that the slower weathering of clinopyroxene resulted from its better lattice fit with talclike layers, making it easier to form a transport-limiting surface product on CPX than on OPX. Colin and others (1985) showed that enstatite from Niquelandia, Brazil, weathered twice as rapidly as diopside to form an homogeneous Fe-saponite matrix. Delvigne (1965) found that orthopyroxene and clinopyroxene from Ivory Coast plutonic rocks reacted differently. In some cases, augite, enstatite, and diopside were directly replaced by iron oxihydroxide septa, leaving a large intersepta porosity. In other cases, only augite was replaced by oxihydroxides, whereas enstatite and diopside, partly hydrothermally altered to chlorite, weathered to a weakly porous matrix composed mainly of chlorite-vermiculite and accessory oxihydroxide. The development of iron oxihydroxide septa was directly related to the parent mineral iron content which reduced the corresponding sizes of intersepta voids. Such septa preserved the texture (fractures, cleavages) of the primary pyroxene. In gabbro from Scotland, the weathering of augite led to the formation of reticulate network-organized vermiculite and amorphous products, leaving voids resulting from congruent dissolution of augite, without formation of any transitional gel phase (Basham, 1974). Hypersthene behaved similarly in the early weathering stages but then differed compared to

augite by being totally weathered into vermiculite and amorphous iron-rich products without void formation (Basham, 1974).

Climatic conditions.—Weathering intensity is much stronger in the tropical humid belt than in cold (Ugolini, 1986) or temperate climates where weathering systems undergo primarily physical processes rather than chemical evolution. Thus, as reported by the literature, tropical conditions offer better opportunities to study the chemical weathering of pyroxenes. The well-known trend is that hot and wet climates enhance smectite genesis, whereas temperate climates favor vermiculite or chlorite-vermiculite (Smith, 1962; Basham, 1974). The direct development of pseudomorphs mimicking the parent mineral, without transitional gel-phase stages are characteristic of chemically less-active systems (Smith, 1962; Basham, 1974). Glasmann (1982) emphasized the importance of climate as a weathering control factor, illustrating the influence of cool-saturated versus warm-unsaturated conditions upon weathering of andesite from Oregon's Western Cascades. The texture of weathered augite (etch pit distribution and denticulated relict crystals) differed greatly from the knobby and irregular surface texture induced by tropical conditions described by Eswaran (1979). In addition, Eswaran (1979) and Glasmann and Simonson (1985) noted that pyroxenes were pseudomorphously replaced by goethite under temperate climates and by hematite and maghemite in weathered basalt under tropical conditions.

Oxygen fugacity conditions.—Oxygen fugacity plays an important role in controlling the precipitation of iron-oxides and oxihydroxides from weathering solutions. Pyroxene dissolves more rapidly during air-excluding experimental weathering (very low values of pO_2) as mentioned by Siever and Woodford (1979). Under high-oxygen conditions, Glasmann (1982) suggested that iron-oxihydroxide precipitated and formed a surface barrier that prevented further congruent dissolution of remnant pyroxene protected in such a way. Velbel (1992) contradicted this hypothesis demonstrating that there was not enough iron, even in endmember Fe-pyroxene, to form a continuous uninterrupted layer of any Fe-oxide or Fe-oxi-hydroxide to protect remnant pyroxene under any conditions. In fact, most petrological evidences showed that dissolution of remnant pyroxenes was not inhibited by the presence of septa and that intersept a high microporosity was preserved during weathering.

Drainage conditions.—Drainage is the most important factor in controlling weathering of pyroxenes at the scale of the mineral as well as at the scale of weathering profiles and landscapes. The intensity of fracturing of fresh and weathered rocks, permeability, flushing rate of water, and amount of percolating water may drastically influence weathering.

Eggleton and Boland (1982) studied the pathways of fluid accessibility to pyroxene. They show that cleavages or lattice defects were the first entry pathways of aqueous solutions into crystals. Such passages increased the weathering rate by enlarging the mineral surface area (Eggleton, 1986).

In closed systems, near line, edge, or screw dislocations, restricted fluid flow and increased residence time enhance rock-solution equilibrium, and consequently, dissolution processes are limited whereas diffusion processes are promoted. In such a case, the parental structure is disrupted only at a local scale, and the so-called "topotactic" replacement by weathering products nucleates from pyroxene surface, keeping crystallographic continuities between primary and secondary phases. Such reactions are also induced by good crystallographic fits between primary and secondary phases.

In contrast, primary minerals dissolve more rapidly where cracks make the weathering system more open to aqueous solution. Such a process can generate, but not always, the loss of parental structures and then induces crystallographic discontinuities with weathering products (Eggleton, 1986; Velbel, 1989; Le Gleuher and Noack, 1990).

According to Smith (1962) the weathering stages of augite depend upon the rate of leaching. Under very intense leaching conditions, both pyroxene and plagioclase dissolve congruently. A less intense leaching will not affect plagioclases, and "the necessary products for clay formation tend to be concentrated into augite" (Smith, 1962, p. 207).

Leaching is also responsible for pH values of weathering solutions by releasing alkaline earth elements. Saponite formation is favored by high pH in medium-grain size rocks, whereas vermiculite exceeds saponite in soils (Smith, 1962).

Delvigne (1965) showed that iron hydroxide septa developed directly from pyroxene under high drainage conditions, whereas transitional phyllosilicates formed within low drainage systems. The size and shape of conducting channels within the weathering profile in the immediate vicinity of the parent-mineral relict determined the course of weathering (Eswaran, 1979).

Pion (1979) reported that weathering products of pyroxenes within gabbro from Kolel (Burkina Faso) range from chlorite through smectites to goethite with increasing drainage conditions. The formation of chlorite, however, can be related to a precursor hydrothermal episode.

Based on samples of basalt in Oregon, Glasmann (1982, p. 255) concluded that augite weathering showed a strong relationship to the proximity of transmineral porosity. He saw that strong dissolution took place when rocks were very porous and when porosity affected augite crystals. Fluids movements were important and facilitated removal of dissolved constituents. He observed however that neighboring pyroxene surrounded by weathered matrix devoid of obvious secondary porosity may show slight pellicular weathering. He said that within these basalts the formation of smectite versus halloysite was favored by restrictive drainage conditions. According to Glasmann (1982, p. 261), "Smectite forms in the altering (weathering) lithic fragments due to the favorable chemical microenvironment whereas halloysite forms in the adjacent soil material." Eventually, these smectites were further transformed to halloysite if the microenvironment underwent more intense leaching. Glasmann and Simonson (1985, p. 272) concluded: "The mineralogy of

the authigenic clay is dependent upon the microchemistry of the weathering environment and may change over a few tens of microns in response to such factors as increased permeability and leaching associated with microcracks." Similar conclusions were given also by De Kimpe, Dejou, and Chevalier (1987).

In an investigation, from the landscape scale to the atomic scale, of the weathering development of Ni-products from Ni-depleted pyroxenite from Niquelandia, Brazil, Colin (1985) and Colin and others (1990) pointed out the role of crack density and drainage conditions in weathering pattern evolution. The parent rock consists of 69 percent OPX (En86), 27 percent CPX (En47Fs4Wo49), and minor chromite. Petrological, mineralogical, and geochemical studies showed that both porosity and fracturing of parent rock influenced genesis of authigenic phases and secondary mineral assemblages. Where fractures were relatively sparse, 50 to 150 μm wide zones of phyllosilicate matrix developed from pyroxenes. This matrix, analyzed by microprobe (table 2), consists of two

TABLE 2

Average structural formula, on a 22 O basis of clay minerals from Jacuba and Angiquinho, Brazil (after Colin, 1985)

	Si	Al	Fe3+	Mg	Ni	Cr	Ti	Ca	K	N
Jacuba										
S1	3.223	0.775	0.964	0.232	1.521	0.078	0.007	0.054	0.015	23
S2	3.420	0.473	1.277	0.290	1.070	0.060	0.003	0.076	0.003	3
T	3.833	0.076	0.353	2.304	0.345	0.027				2
S	3.796	0.439	0.767	0.464	1.002	0.064	0.010	0.017		3
P	4.009	0.001	0.174	0.155	2.508	0.013	0.009	0.009	0.007	3
J1	3.671	0.425	0.358	0.121	2.138	0.093	0.009	0.13	0.047	32
J2	3.660	0.681	0.545	0.173	1.263	0.175	0.013	0.036	0.065	14
J3	3.767	0.718	0.725	0.179	0.902	0.098	0.012	0.020	0.059	9
J4	3.634	0.641	1.030	0.242	0.737	0.117	0.007	0.027	0.056	14
J5	3.684	0.959	0.687	0.214	0.623	0.178	0.016	0.014	0.024	10
K	2.027	1.656	0.101	0.055	0.157	0.044				4
Angiquinho										
A1	3.411	0.656	0.739	1.181	0.631	0.116	0.006	0.069	0.018	9
A2	3.353	1.117	0.962	0.192	0.619	0.115	0.006	0.129	0.047	3
A3	3.345	0.596	0.883	1.243	0.653	0.122	0.004	0.003	0.004	2
A4	3.842	0.507	1.147	0.399	0.286	0.087	0.008	0.003	0.001	6
A5	3.766	0.558	1.237	0.396	0.242	0.072	0.012	0.002	0.007	3
A6	3.844	0.994	0.535	0.348	0.279	0.217	0.031	0.002	0.004	8

Jacuba: S1 and S2 = smectite from weakly fractured coherent rock; T = talc; S = smectite from highly fissured, coherent rock; P = pimelite from high fissuring, coherent rock; J1 = smectite from pyroxene core in coarse saprolite; J2 = smectite from pyroxene rim in coarse saprolite; J3 = smectite from pyroxene core in coarse/argillaceous saprolite; J4 = smectite from pyroxene rim in argillaceous saprolite; J5 = smectite from pyroxene core in argillaceous saprolite; K = kaolinite.

Angiquinho: A1 and A2 = smectites from coarse saprolite; A3 and A4 = smectites from argillaceous saprolite, with conservation of structure; A5 and A6 = smectites from argillaceous saprolite, without conservation of structure.

N = number of analyses.

generations of trioctahedral smectites and minor talc (Colin and others, 1985). Where fracturing was more intense, clay replacement was much better developed and filled embayments developed from pyroxenes. The latter occurred as residual fragments, still preserving their original orientation. XRD and microprobe analyses identified the weathering matrix as a mixture of smectite, pimelite, and minor quartz (table 2).

The paramount role of drainage was also illustrated at the scale of the mineral by the detailed petrological study of pyroxene weathering at Jacuba and Angiquinho (Colin, 1985). Within the coarse saprolite layer, weathering products differed at the rim and in the core of pyroxene. In the center of pyroxene, under low drainage conditions, pyroxene was pseudomorphously replaced by saponite having a low Al content. At the rim, increasing fluid accessibility led to the formation of a saponite richer in Fe-Al (table 2 and fig. 1).

As the weathering system becomes progressively more open to aqueous solutions upward in the profile, smectite evolved from saponite through hisingerite and beidellite to kaolinite, which are Fe-rich at the rim of pyroxene and Al-rich in the center (table 2 and figs. 1 and 2) (Colin, 1985). Weathering processes are characterized by the development of weathering products progressively richer in Al.

Elsewhere the weathering endmember smectites were rather Fe-rich than Al-rich. For example, the pyroxenite of Sipilou in the Ivory Coast weathers to low-temperature talc, as confirmed by oxygen isotope study (Noack, Decarreau, and Manceau, 1986) at the base of the profile, and

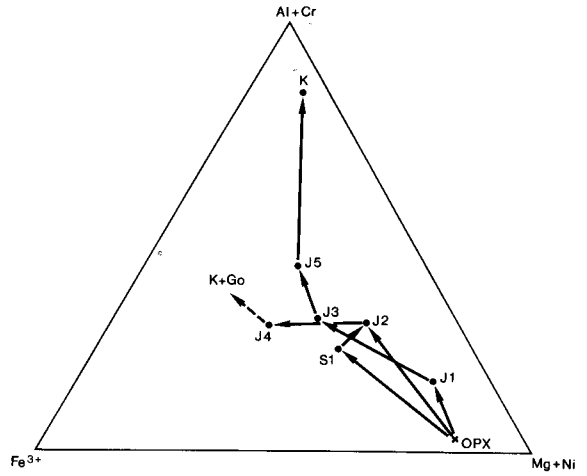

Fig. 1. Evolution of smectites from Jacuba, Brazil (after Colin, 1985) in a Al + Cr/Mg + Ni/Fe^{3+} diagram. OPX = orthopyroxene; S1 = smectite from weakly fractured coherent rock; J1 = smectite from pyroxene core in coarse saprolite; J2 = smectite from pyroxene rim in coarse saprolite; J3 = smectite from pyroxene core in coarse/argillaceous saprolite; J4 = smectite from pyroxene rim in argillaceous saprolite; J5 = smectite from pyroxene core in argillaceous saprolite; K = kaolinite; Go = goethite.

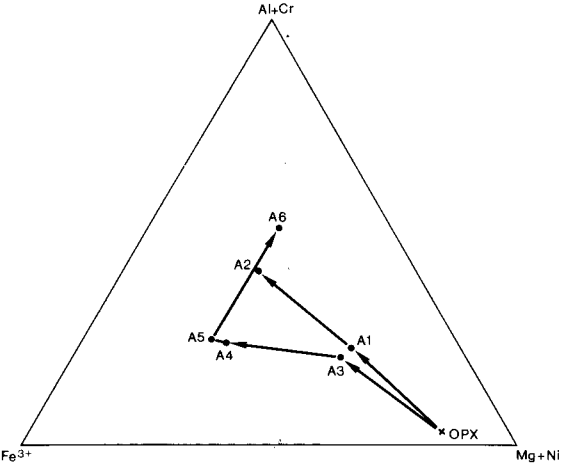

Fig. 2. Evolution of smectites from Angiquinho, Brazil (after Colin, 1985) in a Al + Cr/Mg + Ni/Fe^{3+} diagram. QPX = orthopyroxene; A1 and A2 = smectites from coarse saprolite; A3 and A4 = smectites from argillaceous saprolite, with conservation of structure; A5 and A6 = smectites from argillaceous saprolite, without conservation of structure.

then upward to goethite through transitional saponite and nontronite (fig. 3A), without intermediate kaolinite formation (Nahon and Colin, 1982; Nahon, Paquet, and Delvigne, 1982; Paquet and others, 1983).

Weathering paths of lherzolite from the Pernes Massif in France (Fontanaud, 1982; fig. 3B), of pyroxenite from Koua Bocca in the Ivory Coast (Delvigne, 1983; fig. 3C) and from Australia (Eggleton and Boland, 1982; fig. 3C) show out that Fe or Al-endmember smectite formation was probably controlled by oxygen fugacity and pH changes with respect to drainage rather than by parent mineral composition.

Summary of the Review

Experimental works and electron microscope studies of natural samples showed that the first weathering stage was the formation of an hydrated, Mg or Ca depleted, poorly crystallized layer. This layer was susceptible to detachment from parental pyroxene by ultrasonic treatment and hence was distinct from protonated layers.

Drainage conditions that prevailed in natural profiles are the most important constrains in weathering.

Closed systems favored topotactism. Low drainage conditions, prevailing within the lower part of the weathering profile, induced phyllosilicate formation (mainly saponite). With increasing drainage, phyllosilicates evolved from 2:1 structures, with low tetrahedral charge (saponite), through 2:1 structures, with high tetrahedral charge (beidellite, hisingerite), and finally to 1:1 structures (kaolinite). Phyllosilicate composition ranged from a Mg-endmember to a Fe- or Al-endmember. Under very intense leaching conditions, such as near surface conditions dominating

the upper part of the weathering profile, goethite formed directly at the expense of fresh pyroxene remnants, while earlier formed 2:1 phyllosilicates were gradually replaced by Al-smectites and even by goethite.

Composition of weathering solutions, pH, or oxygen fugacity values were generally not measured in the field and not given in the literature. Results of thermodynamic simulation presented below show the influence of solution composition as a control factor of this evolution toward Al- and Fe-endmembers.

THERMODYNAMIC SIMULATIONS

Thermodynamic Model

The thermodynamic model used was that developed by Fritz (1975, 1981, 1985). It consists of computerized calculations that track the theoretical congruent dissolution, without kinetic effects, of a known mixture of minerals by a specific solution under given conditions, such as starting pH, oxygen, and carbon dioxide fugacities, temperature, and open or closed systems. The state of dissolution was determined by the quantity of starting minerals (in moles) dissolved by 1 kg of solution (=molality; "log m"). Calculations allowed simulation of the chemical evolution of the solution during dissolution of so-called parent minerals. At each time-step of the theoretical dissolution-precipitation simulation, the quantities of dissolved and precipitated minerals were calculated. Secondary minerals were stable in the so-called "open system conditions," but they may redissolve under "closed system conditions" if becoming unstable again. The simulation ended when final chemical steady state was reached (all reactants at equilibrium).

In this study, closed system and fixed gas fugacities were chosen. Primary minerals dissolved congruently at the same rate, and quartz was replaced by amorphous silica. The log K values at 25°C of the primary minerals and of the chosen secondary minerals are given in table 3. The model allowed thermodynamic calculations with solid solution endmembers, considered ideal mixtures of pure endmember phases (Tardy and Fritz, 1981; Fritz, 1985), made this computerized model applicable to natural conditions. Four talc endmembers (1) and 16 mica endmembers (2) were taken into account for smectite solid solutions:

$$Si_4(Al_2, Fe_2^{3+}, Fe_3^{2+}, Mg_3)O_{10}(OH)_2 \quad (1)$$

$$Si_3Al(Al_2, Fe_2^{3+}, Fe_3^{2+}, Mg_3)(Mg_{.5}, Ca_{.5}, Na, K)O_{10}(OH)_2 \quad (2)$$

The beginning of the simulation reflected conditions at the top of the weathering profile, with very dilute solution and high fluid/solid ratio. The end of the simulation corresponded to the base of the profile, with concentrated solution and low fluid/solid ratio. Studies of natural profiles are related to the solid reference frame and investigate weathering sequences from base to top under weathering that is weak at the bottom and intense at the top. On the other hand, simulations are related to the

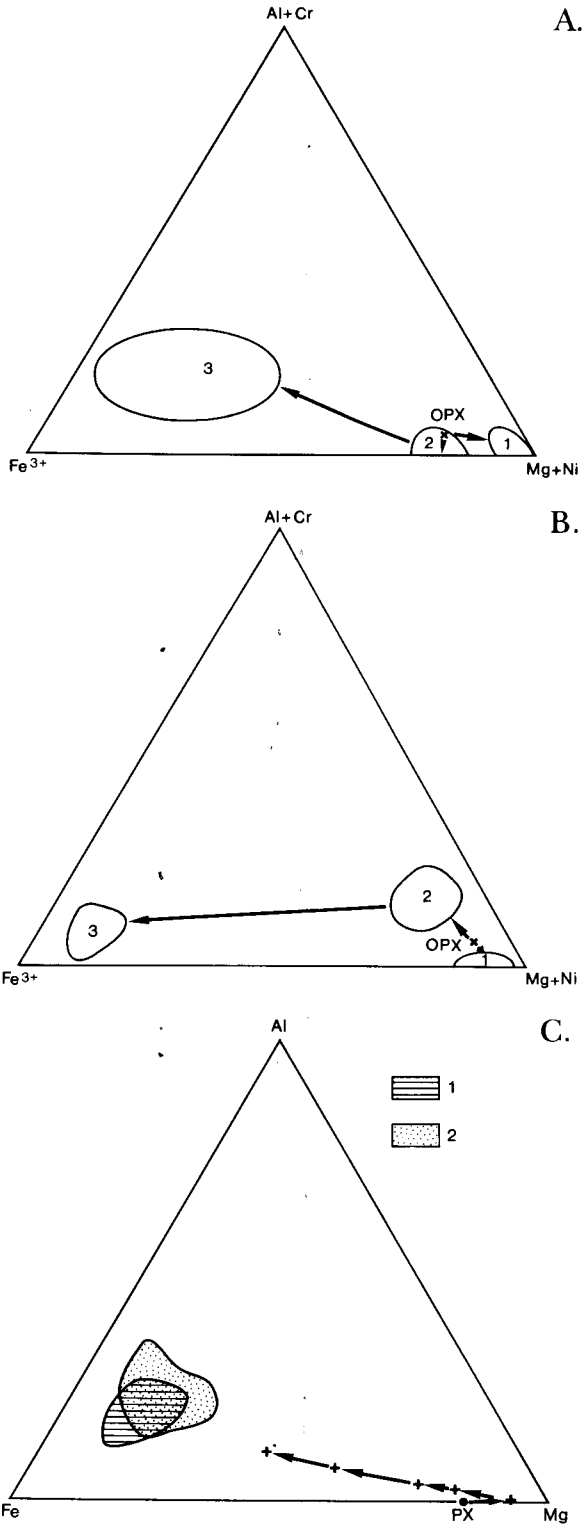

Figure 3

TABLE 3

Thermodynamic data, at 25°C, used for computerized modelization (after Fritz, 1981 and Michaux, ms)

Amorphous silica	−2.714	Greenalite	17.541
Annite	23.273	Grunerite	34.312
Annite-Ca	24.006	Hematite	1.692
Annite-Mg	24.006	Kaolinite	7.410
Annite-Na	24.079	Magnesite	−8.040
Anthophyllite	67.787	Magnetite	3.826
Brucite	−11.210	Minnesotaite	7.235
Calcite	−8.370	Muscovite	16.656
Chlinochlore	68.560	Muscovite-Ca	17.389
Chrysotile	32.200	Muscovite-Mg	17.389
Daphnite	45.550	Muscovite-Na	17.462
Enstatite	11.360	Phlogopite	41.913
Epidote	31.060	Phlogopite-Ca	42.646
Ferrimuscovite	27.148	Phlogopite-Mg	42.646
Ferrimuscovite-Ca	27.881	Phlogopite-Na	42.719
Ferrimuscovite-Mg	27.881	Pyrophyllite	1.061
Ferrimuscovite-Na	27.954	Pyrophyllite-Fe3	14.028
Ferrosilite	5.850	Pyroxene-Ca-Al	36.460
Ferrotremolite	36.115	Talc	25.162
Gibbsite	8.230	Tremolite	61.670
Goethite	0.819	Zoizite	43.958

fluid reference frame and pertain to solutions that are dilute at the top and concentrated at the bottom.

Parent Mineral

Weathering of orthopyroxene and clinopyroxene (whose formulae are respectively [$Si_{0.98}Al_{0.04}Fe_{0.34}Mg_{0.62}Ca_{0.02}O_3$) and $Si_{1.96}Al_{0.08}Fe_{0.24}Mg_{0.84}Ca_{0.88}O_6$]) was simulated in the following system, which mostly reflects natural conditions:

T = 25°C, fixed $pO_2 = 10^{-30}$ atm, fixed $pCO_2 = 10^{-3.5}$ atm

Initial pH = 5.6, Initial Eh = 454mV

Initial (Si, Al, Fe, Mg, Ca, Na) = 10^{-9} mole/l.

These conditions are approximately those of natural rain waters.

Secondary minerals precipitated sequentially in the following order (fig. 4):

—OPX dissolution: goethite, gibbsite, kaolinite, Fe-Mg-smectite, Mg-serpentine, tremolite;

Fig. 3(A) Evolution of smectites from Sipilou, Ivory Coast (after Nahon, Paquet, and Delvigne, 1982 and Paquet and others, 1983) in a Al + Cr/Mg + Ni/Fe^{3+} diagram. OPX = orthopyroxene; 1 = talc; 2 = saponite; 3 = nontronite.

(B) Evolution of smectites from Pernes, France (after Fontanaud, ms; and Fontanaud and Meunier, 1983) in a Al + Cr/Mg + Ni/Fe^{3+} diagram. OPX = orthopyroxene; 1 = talc; 2 = saponite; 3 = nontronite.

(C) Evolution of smectites from Koua Bocca, Ivory Coast (after Delvigne, 1983) and from Australia (Eggleton and Boland, 1982) in a Al + Cr/Mg + Ni/Fe^{3+} diagram. 1 = smectites from orthopyroxene (Koua Bocca); 2 = smectites from clinopyroxene (Koua Bocca). PX = orthopyroxene from Australia; crosses = evolution of smectites from Australia during weathering.

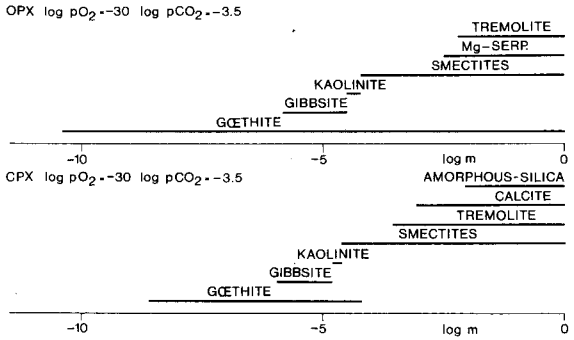

Fig. 4. Modeling of pyroxene dissolution. Evolution of secondary minerals with orthopyroxene (OPX) and clinopyroxene (CPX) dissolution (log m) (after Michaux, ms).

—CPX dissolution: goethite, gibbsite, kaolinite, Fe-Mg-smectite, tremolite, calcite, amorphous silica.

Gibbsite (in small amounts from OPX), kaolinite, and CPX-derived goethite precipitated and dissolved during the simulations (close system effect). Except for goethite, the precipitation of secondary phases was reached at lower log m values for CPX than for OPX, that is, at a less evolved dissolution state. Amounts and chemical compositions of ortho- and clinopyroxene-derived smectites differed (figs. 5 and 6). Smectites accounted for 80 percent when one mole of OPX was dissolved and evolved from iron endmember to magnesium endmember when tetrahedral charge decreased from 1 to 0.2 (fig. 7). In the first stage of smectite formation, ferri-muscovite accounted for 84 percent (table 4). When the solution was saturated with respect to tremolite, talc (65 percent) and pyrophyllite (17 percent) formed as Mg- and Fe^{3+} endmembers respectively. For CPX, smectite minerals represented 20 percent in volume of the total secondary phases. The first smectites formed were close to ferri-muscovite endmembers and accounted for 91 percent of the total smectites. As the simulation proceeded, Ca-endmember smectite represented 58 percent of the total volume and was always a ferri-muscovite; the Mg-ferri-muscovite contribution (6 percent) decreased at the benefit of ferri-pyrophyllite (34 percent) (table 4). The tetrahedral charge was high (> 0.5).

At the end of the simulation, that is, under very closed system conditions, serpentine and tremolite formed after OPX, whereas tremolite, calcite, and amorphous silica developed after CPX. Under natural conditions, these minerals are generally believed to originate from hydrothermal alteration or metamorphism. In the case of OPX weathering simulation, serpentine and tremolite formation was accompanied by an increase of 10 percent in volume. Such volumetric expansion does not take place under natural weathering conditions. We believe that the

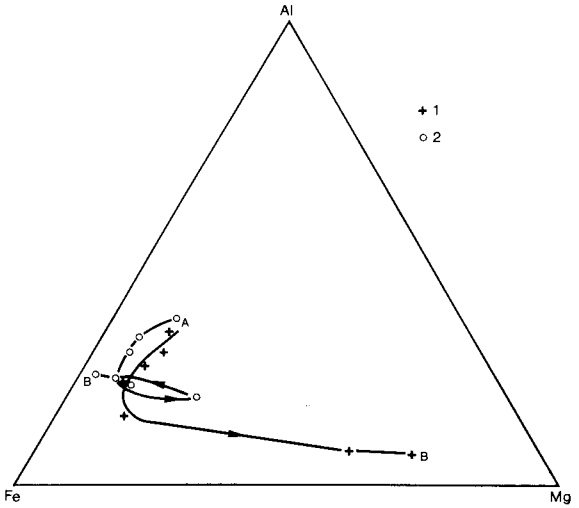

Fig. 5. Modeling of pyroxene dissolution. Evolution of smectite composition for orthopyroxene (1) and clinopyroxene (2) in a Al-Fe-Mg diagram. A = beginning of modelization; B = end of modelization (after Michaux, ms).

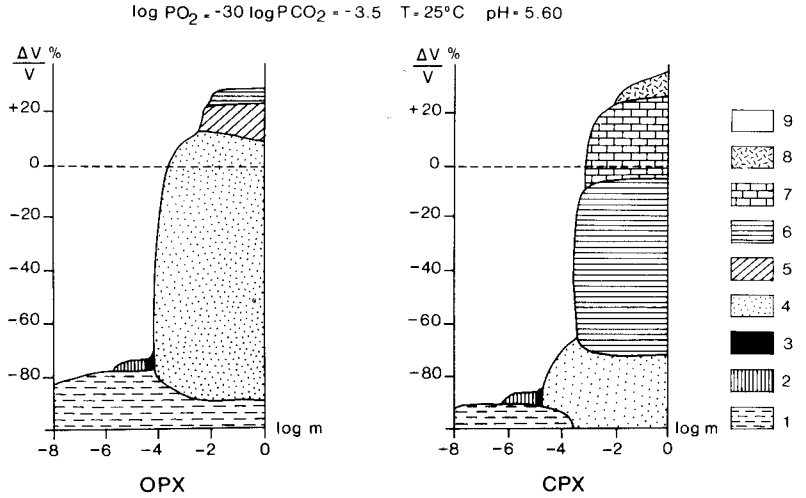

Fig. 6. Modeling of pyroxene dissolution. Evolution of the secondary minerals volumes during pyroxene dissolution (log m). OPX = orthopyroxene; CPX = clinopyroxene; 1 = goethite; 2 = gibbsite; 3 = kaolinite; 4 = smectites; 5 = serpentine; 6 = tremolite; 7 = calcite; 8 = amorphous silica; 9 = void/porosity (after Michaux, ms).

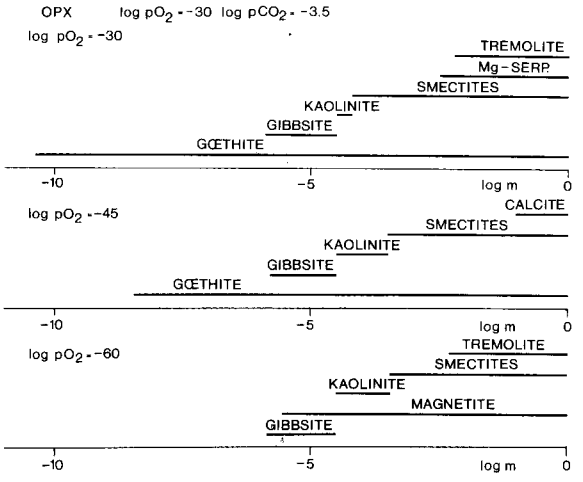

Fig. 7. Modeling of pyroxene dissolution. Evolution of secondary minerals with orthopyroxene dissolution (log m) at different oxygen fugacity (after Michaux, ms).

necessary solution composition to precipitate amphiboles is never reached in natural profiles. The composition of the weathering solution evolves with depth and is successively in equilibrium with iron and aluminum hydroxides, kaolinite, and smectites.

When equilibrium with smectites was reached, the precipitation of these minerals was associated with a volume increase which can reduce porosity and restrict fluid circulation. Consequently, the composition of the solution could not evolve any further, and equilibrium with amphiboles was never reached. In regard to the weathering of CPX, tremolite appeared when porosity was still important (70 percent). Two hypotheses were proposed: (1) the precipitation rate of amphiboles at low

TABLE 4

Distribution of smectite solid-solution endmembers, at different stages of pyroxene dissolution

		Talc	Min.	Pyro. Al	Pyro. Fe3	Musc. Mg	Musc. Ca
OPX	First Smec.	0.00	0.00	0.62	0.03	4.72	0.80
log pO2 = −30	Trem. sat.	65.54	0.00	0.00	17.21	0.00	0.00
OPX	First Smec.	1.56	1.22	22.22	0.00	61.3	10.79
log pO2 = −60	Trem. sat.	83.60	2.22	2.71	0.00	0.52	0.28
	First Smec.	0.00	0.00	0.42	0.02	3.91	4.01
CPX	Trem. sat.	4.93	0.00	0.00	31.70	0.00	0.00
log pO2 = −30	Silica sat.	1.25	0.00	0.38	33.56	0.00	0.00

Abbreviations: Min. = Minnesotaite. Pyro. = Pyrophyllite. Musc. = Muscovite. Phlog. = Phlogopite. Smec. = Smectite. Trem. = Tremolite.

temperature was slow, and the formation of smectite minerals was favored; (2) in studied natural profiles, CPX was always mixed with OPX, which is the more important phase, and the situation described by the simulation was never observed.

Whereas initial chemical compositions of the solutions were similar during both OPX and CPX dissolution simulations, they differed only in the final stage. When calcite saturation was reached for CPX, aluminum activity increased and magnesium activity strongly decreased. At the end of the simulation, silica activity was higher for CPX than for OPX. Smectite saturation was obtained for approximately the same cation activities.

Oxidizing Conditions

The weathering of OPX was simulated under three different conditions, as follows:

1. fixed $pO_2 = 10^{-30}$ atm, initial pH = 6.44, initial Eh = 404 mV;
2. fixed $pO_2 = 10^{-45}$ atm, initial pH = 5.60, initial Eh = 232 mV,
3. fixed $pO_2 = 10^{-60}$ atm, initial pH = 5.60, initial Eh = 106 mV.

In the second simulation, tremolite was not tested but replaced by carbonate. The results obtained indicate the following order of secondary phases formation (fig. 8):

1. Goethite, gibbsite, kaolinite, Fe-Mg-smectite, Mg-serpentine, tremolite;
2. Goethite, gibbsite, kaolinite, Fe-Mg-smectite, calcite;
3. Gibbsite, magnetite, kaolinite, Fe-Mg-smectite, tremolite.

With decreasing oxygen fugacity, secondary phases precipitated from increasingly dissolved pyroxene. The same minerals are found, except with the lowest fugacity where goethite was replaced by magnetite. The stability field of kaolinite enlarged as oxygen fugacity decreased.

The chemical composition of the smectite solid solution was strongly influenced by oxygen fugacities. The final bulk composition was in any case close to the Mg-endmembers, approximating pyroxene composition

TABLE 4
(continued)

		Fe-Musc. Mg	Fe-Musc. Ca	Annite Mg	Annite Ca	Phlog. Mg	Phlog. Ca
OPX	First Smec.	80.20	13.61	0.00	0.00	0.00	0.00
log pO2 = −30	Trem. sat.	12.00	5.27	0.00	0.00	0.00	0.00
OPX	First Smec.	4.45	0.78	0.12	0.02	0.00	0.00
log pO2 = −60	Trem. sat.	5.66	2.99	0.15	0.08	1.12	0.59
	First Smec.	45.29	46.34	0.00	0.00	0.00	0.00
CPX	Trem. sat.	19.64	43.75	0.00	0.00	0.00	0.00
log pO2 = −30	Silica sat.	6.64	58.20	0.00	0.00	0.00	0.00

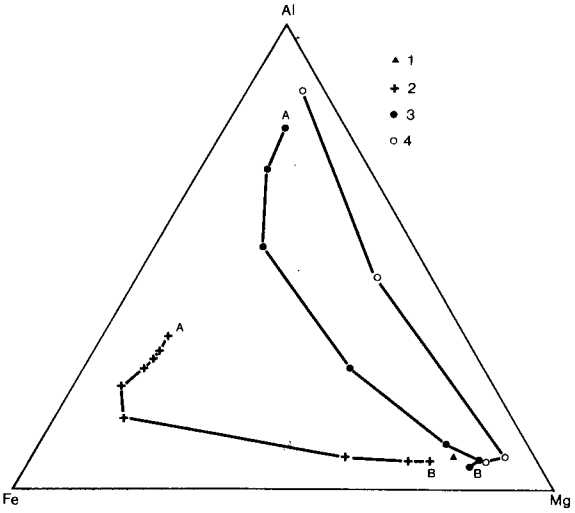

Fig. 8. Modeling of pyroxene dissolution. Evolution of smectite composition during orthopyroxene (1) dissolution, at different oxygen fugacity in a Al-Fe-Mg diagram. (2) log $pO_2 = -30$; (3) log $pO_2 = -45$; (4) log $pO_2 = -60$ (A) = beginning of the modelization; (B) = end of the modelization (after Michaux, ms).

(fig. 9). However, endmembers were distributed slightly differently as oxygen fugacity changed. At the highest fugacity, talc accounted for 65 percent and ferri-pyrophyllite for 18 percent of the total volume of secondary phases. At the lowest fugacity, talc contribution increased to 86 percent and the volume of pyrophyllite and ferri-muscovite decreased (table 4). The chemical composition of the first smectite mineral to precipitate (fig. 9) and the evolution of aqueous solution varied according to oxygen fugacity. At the lower fugacity, the smectite was Al-rich and muscovite endmembers accounted for 82 percent of the total volume. The first smectites formed under high silica and magnesium activities as oxygen fugacity was reduced. At the end of the simulation, at log $pO_2 = -30$, silica activity decreased and then increased again to reach the value of log $(H_4SiO_4) = -3$ for log $pO_2 = -60$ atm.

Comparison with Natural Profiles

Goethite and gibbsite modeled during the first steps of simulations can be compared to similar weathering products developed at the top of weathering profiles (if unweathered pyroxenes are preserved) under well drained and open system conditions. In the same way, simulated smectite formation approximated natural smectite development at the water table front under reduced oxygen fugacity and closed system conditions. Chemical compositions of smectite solid solutions were generally in good agreement with natural smectite compositions. Mg-bearing trioctahedral smectites having low tetrahedral charges formed at the end

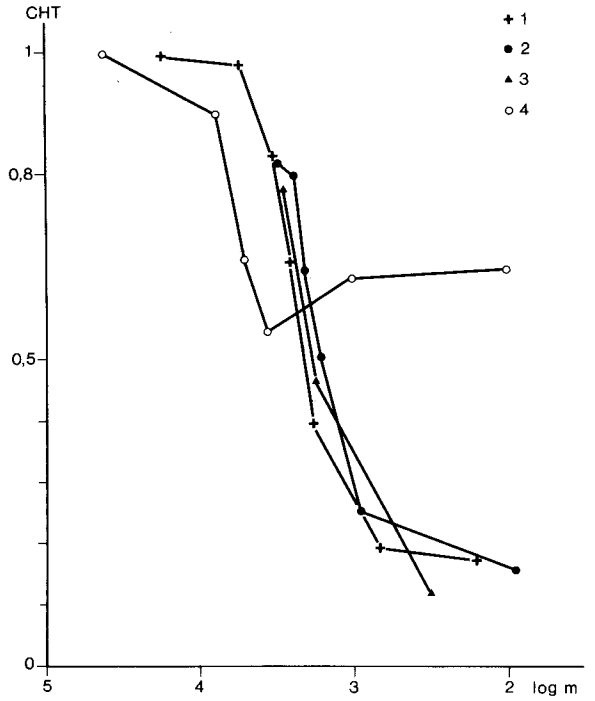

Fig. 9. Modeling of pyroxene dissolution. Evolution of smectite tetrahedral charge during pyroxene dissolution (log m), at different oxygen fugacity. (1) OPX, log $pO_2 = -30$; (2) OPX, log $pO_2 = -45$; (3) OPX, log $pO_2 = -60$; (4) CPX, log $pO_2 = -30$ (after Michaux, ms).

of the simulation (base of profiles), whereas iron rich smectites (oxidizing conditions) and aluminum rich smectites (reducing conditions) were calculated to precipitate at the beginning of the experiments (top of profiles). These smectites are found in natural weathering as shown in figures 1 and 2. The chosen value of $pO_2 = 10^{-30}$ atm corresponds to well-ventilated weathering profiles and may promote the formation of iron-rich smectites. In contrast, 10^{-60} atm is not comparable to natural conditions; therefore the formation of aluminum-rich smectites, as for example within Jacuba and Angiquinho profiles (figs. 1 and 2), can only be explained by high aluminum contents of parent minerals. Proust (ms) showed that amphibole weathering leads to Al-rich smectites. Furthermore, short-distance transfer of aluminum during weathering of neighboring minerals can also induce the formation of Al-rich smectite such as beidellite (Nahon, Colin, and Tardy, 1982; De Kimpe, Dejou, and Chevalier, 1987). Such factors were tested by simulations for which starting aqueous solutions were enriched in aluminum with three stages representing gibbsite, kaolinite, and albite saturation (figs. 10 and 11).

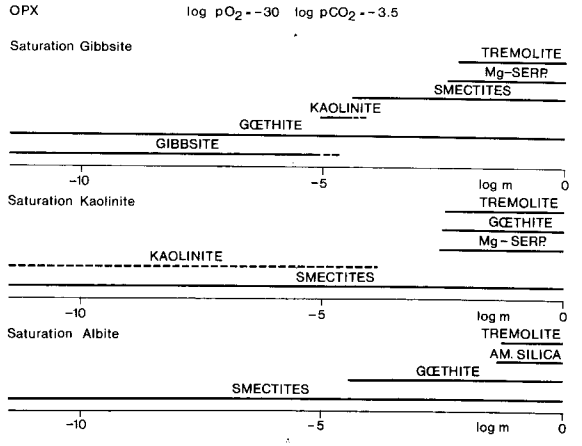

Fig. 10. Modeling of pyroxene dissolution. Evolution of secondary minerals with orthopyroxene dissolution (log m) for different starting solution (after Michaux, ms).

Similar results were obtained from calculations done with pure water and gibbsite saturated solution. From the beginning of the simulations, the two other solutions were saturated with respect to smectite minerals (log m = −10). The secondary minerals were identical to those resulting from

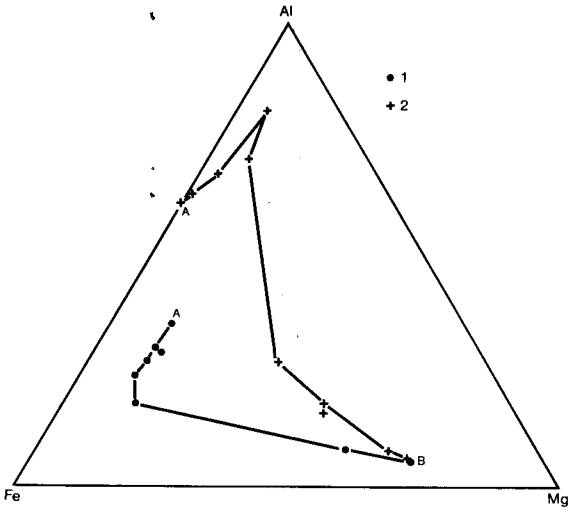

Fig. 11. Modeling of pyroxene dissolution. Evolution of smectite composition for orthopyroxene dissolution, for different starting solution in a Al-Fe-Mg diagram. (1) gibbsite saturation; (2) kaolinite saturation. (A) = beginning of modelization; B = end of modelization.

the standard simulation ($pO_2 = 10^{-30}$, Al = 10^{-9}) and were successively goethite, smectites, tremolite, Mg-serpentine, and amorphous silica (fig. 10). The composition of the smectites differed for kaolinite- or albite-saturated solution. In the first case, smectites evolved from Fe-Al to Al-rich smectites as kaolinite dissolved and subsequently to Mg-rich smectites (fig. 11). In the second case, smectites evolved from Al to Mg-rich smectites (fig. 11). In the first stages of smectite formation, silica activity was higher, and magnesium and aluminum activities were lower in the solution. By comparing smectite composition diagrams with those obtained for Brazilian samples (figs. 1 and 2), we concluded that external Al-contamination with respect to the parent pyroxene crystal induced Al-smectite formation within these natural weathering profiles. Mass balance calculations indicated that weathered rocks of Jacuba and Angiquinho, respectively, lost and gained aluminum with respect to parent rock (Colin, 1985; Colin and others, 1990). At Jacuba, pseudomorphic smectite is Al-enriched relative to pyroxene, and such aluminum can be supplied by the crystal-scale weathering of coexisting minerals. At Angiquinho, aluminum may originate in the landscape-scale weathering of surrounding rocks such as anorthosite and amphibolite.

CONCLUDING REMARKS

Our review of literature data on pyroxene weathering showed that drainage conditions are the most important factor in controlling weathering processes and in determining the sequence of secondary minerals. But, factors such as weathering solution composition, pH value, pO_2 value, which are difficult to collect or to measure (whether in the field or in the laboratory), are believed to be important. Computerized thermodynamic models are useful tools to test the effects of varying initial conditions on the weathering process. Our calculations showed that pO_2 variations have a strong effect on the composition of the clay solid-solution. At average pO_2 (near atmospheric equilibrium), in pure water, the solid-solution evolved from a Mg-rich to a Fe-rich endmember. At very low oxygen fugacity, smectite solid-solution evolved into an Al-rich endmember. But the same effect can be obtained with an average oxygen fugacity and a high aluminum content of the weathering solution.

Thermodynamic modeling results are generally consistent with natural weathering paths. However, computerized and natural pyroxene-derived secondary products may have quite different origins. Under thermodynamic modeling conditions, enough pyroxene is always available to allow its transformation into successive secondary products of varying composition. In contrast, within most of the natural weathering mantles, pyroxenes were totally replaced by smectites at the base of the profile, and hence, no pyroxene remnants were available for further weathering into kaolinite. In this case, kaolinite resulted from the weathering of former smectites under different physico-chemical conditions than those prevailing in the thermodynamic model.

The next critical step to improve predictive simulations of pyroxene dissolution and, more generally, of primary silicate dissolution and the formation of secondary products is to take into account kinetic effects with different sets of initial conditions. In addition, analysis of weathering solutions and measurement of oxygen fugacity in natural conditions are a critical requirement to bring simulation and natural approach into better agreement.

Acknowledgments

This work has been supported by CNRS program Dynamique et Bilan de la Terre (contribution number 408). The authors are grateful to M. A. Velbel and B. Fritz for their reviews of this paper and to A. J. Carozzi for the English grammar and syntax.

References

Basham, I. R., 1974, Mineralogical changes associated with deep weathering of gabbro in Aberdeenshire: Clay Minerals, v. 10, p. 189–202.

Berner, R. A., and Schott, J., 1982, Mechanism of pyroxene and amphibole weathering: II observations of soil grains: American Journal of Science, v. 282, p. 1214–1241.

Berner, R. A., Sjöberg, E. L., Velbel, M. A., and Krom, M. D., 1980, Dissolution of pyroxenes and amphiboles during weathering: Sciences, v. 207, p. 1205–1206.

Colin, F., ms, 1985, Etude pétrologique des altérations de pyroxénite du gisement nickelifere de Niquelandia (Brésil): Thèse 3ème Cycle, T. D. M. ORSTOM, Edition de l'ORSTOM, Paris, 137 p.

Colin, F., Nahon, D., Trescases, J-J., and Melfi, A. J., 1990, Lateritic weathering of pyroxenites at Niquelandia, Goias, Brazil: the supergene behavior of nickel: Economic Geology, v. 85, p. 1010–1023.

Colin, F., Noack, Y., Trescases, J-J., and Nahon, D., 1985, L'altération latèritique débutante des pyroxénites de Jacuba, Niquelandia (Bresil): Clay Minerals, v. 20, p. 93–113.

De Kimpe, C., Dejou, J., and Chevalier, Y., 1987, Evolution géochimique superficielle des pyroxénites ignées du Mt St Bruno, Quebec: Canadian Journal of Earth Science, v. 24, p. 760-770.

Delvigne, J., 1965, Pédogenèse en zone tropical. La formation des minéraux secondaires en milieu ferrallitique: Mémoires ORSTOM, Paris, 13, 177 p.

———— 1983, Micromorphology of the alteration and weathering of pyroxenes in the Koua Bocca ultramafic intrusion, Ivory Coast, Western Africa, *in* Nahon, D., and Noack, Y., editors, Pétrologie des Altérations et des sols: International CNRS Colloquim, Sciences Géologiques, Mémoires, v. 72, p. 57–68.

———— 1990, Hypogene and supergene alterations of orthopyroxene in the Koûa Bocca ultramafic intrusion, Ivory Coast: Chemical Geology, v. 84, p. 49–53.

De Oliveira, S. M. B., and Delvigne, J., 1988, Evolucao mineralogica dos Jacupirangvitos de Jacupiranga (SP) durante a alteracao intemperica: Revista Brasiliera Geosciências, v. 18 no. 1, p. 79–85.

Eggleton, R. A., 1986, The relationships between crystal structure and silcate weathering rates, *in* Colman, S. M., and Dethier, D. P., editors, Rates of Chemical weathering of rocks and minerals: Orlando, Florida, Academic Press Incorporated, p. 21–40.

Eggleton, R. A., and Boland, J. N., 1982, Weathering of enstatite to talc through a sequence of transitional phases: Clays and Clay Minerals, v. 30, no. 1, p. 11–20.

Eswaren, H., 1979, The alteration of plagioclases and augite under differing pedoenvironmental conditions: Journal of Soil Sciences, v. 30, p. 547–555.

Fontanaud, A., ms, 1982, Les faciès d'altération supergene des roches ultrabasiques, Etude de deux massifs de lherzolite (Pyrénées, France): Thèse 3ème cycle, Poitiers, 103 p.

Fontanaud, A., and Meunier, A., 1983, Mineralogical facies of a weathered serpentinized lherzolite from Pyrenees, France: Clay Minerals, v. 18, p. 77–88.

Fritz, B., 1975, Etude thermodynamique et simulations des réactions entre minéraux et solutions. Application à la géochemie des altérations et des eaux continentales: Sciences Géologiques, Mémoires, v. 41, 152 p.

———— 1981, Etude thermodynamique et modélisation des réactions hydrothermales et diagenétiques: Sciences Géologiques, Mémoires, v. 65, 197 p.

———— 1985, Multicomponent solid solutions for clay minerals and computer modeling of weathering processes, *in* Drever, J. I., and Reidel, P. C., editors, Chemistry of weathering: NATO ASI Series C, v. 149, p. 19–34.

Glasmann, J. R., 1982, Alteration of andesite in wet, unstable soil of Oregon's Western Cascades: Clays and Clay Minerals, v. 30, no. 4, p. 253–263.

Glasmann, J. R., and Simonson, G. H., 1985, Alteration of basalt in soils of Western Oregon: Soil Science Society of America, v. 49, p. 262–273.

Grandstaff, D. E., 1977, Some kinetics of bronzite orthopyroxene dissolution: Geochimica et Cosmochimica Acta, v. 41, p. 1097–1103.

Helgeson, H. C., Brown, T. H., Nigrini, A., and Jones, T. A., 1970, Calculation of mass transfer in geochemical processes involving aqueous solutions: Geochimica et Cosmochimica Acta, v. 34, p. 569–592.

Helgeson, H. C., Garrels, R. M., and Mackenzie, F. T., 1969, Evaluation of irreversible reactions in geochemical processes involving minerals and aqueous solutions. II—Applications: Geochimica et Cosmochimica Acta, v. 33, p. 455–481.

Hendricks, D. M., and Whittig, L. D., 1968a, Andesite weathering: I-Mineralogical transformations from andesite to saprolite: Journal of Soil Sciences, v. 19, no. 1, p. 135–146.

———— 1968b, Andesite weathering: II-Geochemical changes from andesite to saprolite: Journal of Soil Sciences, v. 1, p. 147–153.

Ildefonse, P., ms, 1987, Analyse pétrologique des altérations prémetéoriques et météoriques de deux roches basaltiques (Basalte alcalin de Belbex, Cantal et Hawaite de M'Bouda, Cameroun): Thèse es Sciences, Paris, 323 p.

Lartigue, J-E., Benedetti, M., Ambrosi, J-P., and Noack, Y., 1991, Experimental weathering of augite under various pH at 25°C using a mixed flow reactor: Terra Abstracts, v. 3, no. 1, p. 472–473.

Le Gleuher, M., and Noack, Y., 1990, Variété de l'ouralitisation des roches pyroxèniques. Interférence de la composition minerale et de l'ouverture du système d'altération: Compte Rendus de l'Academie des Sciences Paris, v. 311, Serie II, p. 805–811.

Loughnan, F. C., 1969, Chemical weathering of the silicate minerals: New York, American Elsevier Edition, 154 p.

Luce, R. W., Bartlett, R. W., and Parks, G. A., 1972, Dissolution kinetics of magnesium silcates: Geochimica et Cosmochimica Acta, v. 36, p. 35–50.

Madé, B., Clement, A., and Fritz, B., 1990, Modelisation cinétique et thermodynamique de altération: le modèle géochimique KINDIS: Compte Rendus de l'Academie des Sciences Paris, v. 310, Série II, p. 31–36.

Michaux, L., ms, 1988, Altérations supergènes et hydrothermales des roches basiques et ultrabasiques. Pétrologie, géochimie et modélisations thermodynamiques: Thèse Université Aix-Marseille III, 195 p.

Mogk, D. W., and Locke, W. W., 1988, Application of Auger Electron Spectroscopy (AES) to naturally weathered hornblende: Geochimica et Cosmochimica Acta, v. 52, p. 2537–2542.

Nahon, D., and Colin, F., 1982, Chemical weathering of orhtopyroxenes under lateritic conditions: American Journal of Science, v. 282, p. 1232–1243.

Nahon, D., Colin, F., and Tardy, Y., 1982, Formation and distribution of Mg, Fe, Mn-smectites in the first stages of the lacteric weathering of forsterite and tephroite: Clay Minerals, v. 17, p. 339–348.

Nahon, D., Paquet, H., and Delvigne, J., 1982, Lateric weathering of ultramafic rocks and the concentration of nickel in the Western Ivory Coast: Economic Geology, v. 77, p. 1159–1175.

Noack, Y., Decarreau, A., and Manceau, A., 1986, Spectroscopic and oxygen isotopic evidence for low and high temperature origin for talc: Bulletin of Mineralogy, v. 109, p. 253–263.

Paquet, H., Duplay, J., Nahon, D., Tardy, Y., and Millot, G., 1983, Analyses chimiques de particules isolées dans les populations de minéraux argileux. Passage des smectites magnesiennes trioctaèdriques aux smectites ferrifères dioctaèdriques au cours de l'altération des roches ultrabasiques: Compte Rendus de l'Academie des Sciences, v. 296, p. 699–704.

Pavich, M. J., Brown, L., Harden, J., Klein, J., and Middleton, R., 1986, 10Be distribution in soils from Merced River Terraces, California: Geochimica et Cosmochimica Acta, v. 50, p. 1727–1735.

Pavich, M. J., Brown, L., Klein, J., and Middleton, R., 1984, 10Be accumulation in a soil chronosequence: Earth and Planetary Science Letters, v. 68, p. 198–204.

Petit, J-C., Della Mea, G., Dran, J-C., Schott, J., and Berner, R. A., 1987, Mechanism of diopside dissolution from hydrogen depth profiling: Nature, v. 325, p. 705–707.

Pion, J. C., 1979, Altération de massifs cristallins basiques en zone tropicale sèche. Etude de quelques toposéquences en Haute-Volta: Sciences Géologiques, Mémoires, v. 57, 220 p.

Proust, D., ms, 1983, Mécanismes de l'altération supergène des roches basiques. Etude des arènes d'orthoamphibolite du Limousin et de glaucophanite de l'île de Groix (Morbihan): Thèse es Sciences, Poitiers, 200 p.

Savin, S. M., and Lee, M., 1988, Isotope studies of phyllosilicates, *in* Bailey, editor, Hydrous Phyllosilicates (exclusive of micas): Reviews in Mineralogy, v. 19, p. 188–223.

Schott, J., and Berner, R. A., 1983, X-Ray photoelectron studies of the mechanism of iron silicate dissolution during weathering: Geochimica et Cosmochimica Acta, v. 47, p. 2233–2240.

———— 1985, Dissolution mechanisms of pyroxes and olivines during weathering, *in* Drever, J. I., and Reidel, P. C., editors, Chemistry of Weathering: NATO ASI Series, Series C, v. 149, p. 35–53.

Schott, J., Berner, R. A., and Sjoberg, E. L., 1981, Mechanism of pyroxene and amphibole weathering. I-Experimental studies of iron-free minerals: Geochimica et Cosmochimica Acta, v. 45, p. 2123–2135.

Siever, R., and Woodford, N., 1979, Dissolution kinetics and the weathering of mafic minerals: Geochimica et Cosmochimica Acta, v. 43, p. 717–724.

Smith, W. W., 1962, Weathering in some Scottish basic igneious rocks with reference to soil formation: Soil Sciences Journal, v. 13, p. 202–214.

Tardy, Y., and Fritz, B., 1981, An ideal solid solution for calculating solubility of clay minerals: Clay Minerals, v. 16, p. 361–373.

Trescases, J. J., 1975, L'évolution géochemique supergène des roches ultrabasiques en zone tropicale. Formation des gisements nickelifères de Nouvelle-Calédonie: Memoires ORSTOM, Paris, v. 78, 259 p.

Ugolini, F. C., 1986, Processes and rates of weathering in cold and polar desert environments, *in* Colman, S. M., and Dethier, D. P., editors, Rates of Chemical Weathering of Rocks and Minerals: Orlando, Florida, Academic Press Inc., p. 193–235.

Velbel, M. A., 1987, Rate controlling fators in the weathering of some ferromagnesian silicate minerals: International Society of Soil Sciences Congress, 13th, Hamburg, Transactions VI, p. 1107–1118.

———— 1989, Weathering of hornblende to ferruginous products by a dissolution-precipitation mechanism: petrography and stoichiometry: Clays and Clay Minerals, v. 37, p. 515–524.

———— 1992, Parent/product volume relationships during silicate-mineral weathering and the formation of "protective" surface layers: American Mineralogist, in press.

Wolery, T. J., and Walters, L. J., 1975, Calculation of equilibrium distributions of chemical species in aqueous solutions by means of monotone sequences: Mathmatical Geology, p. 99–115.